Targeting the Post-Synaptic Proteome in Alzheimer Disease with Psychosis

Josh Krivinko
University of Pittsburgh
Michael DeChellis-Marks
University of Pittsburgh
Lang Zeng
University of Pittsburgh
Peihao Fan
University of Pittsburgh
Oscar Lopez
Departments of Neurology and Psychiatry, University of Pittsburgh https://orcid.org/0000-0002-8546-8256
Ying Ding
University of Pittsburgh https://orcid.org/0000-0003-1352-1000
Lirong Wang
University of Pittsburgh
Julia Kofler
University of Pittsburgh
Matthew MacDonald
University of Pittburgh
Robert Sweet (sweetra@upmc.edu)
University of Pittsburgh https://orcid.org/0000-0001-9154-9709

Article

Keywords: Alzheimer's Disease, Psychosis, Post-synaptic Density, Proteomics: Systems Pharmacology

Posted Date: April 4th, 2022

DOI: https://doi.org/10.21203/rs.3.rs-1514870/v1

Abstract

Individuals with Alzheimer Disease with psychotic symptoms (AD + P) experience more rapid cognitive and functional decline, and have reduced indices of synaptic integrity, relative to those without psychosis (AD-P). We hypothesized the postsynaptic density (PSD) proteome is altered in AD + P relative to AD-P, and that this proteomic signature could be used to nominate novel pharmacotherapies. Liquid-Chromatography/Mass Spectrometry analysis of PSDs from dorsolateral prefrontal cortex of AD + P, AD-P and cognitively normal elderly subjects. The PSD proteome signature of AD + P was characterized by lower levels of proteins regulating Rho GTPases and the actin cytoskeleton. Potential novel therapies identified included the C-C Motif Chemokine Receptor 5 inhibitor, maraviroc. AD + P is characterized by broad changes in the PSD proteome in prefrontal cortex. Further testing of potential therapies for their ability to reverse these changes and protect against psychotic-like behaviors in model systems is warranted.

Introduction

Psychotic symptoms affect ~ 40–60% of individuals with Alzheimer Disease (AD) [1]. AD subjects with psychosis (AD + P) experience more rapid cognitive decline compared to AD subjects without psychosis (AD-P) [1–4]. Greater cognitive dysfunction in AD + P is present in the earliest disease stages, preceding psychosis onset [2,3]. Current treatment for psychosis in AD with antipsychotics have limited efficacy, do not mitigate the more rapid cognitive decline, and confer excess mortality [5]. As a result, AD + P is associated with worse outcomes than AD-P: aggression [6], caregiver distress [7], functional decline [8], institutionalization [9], and mortality [10]. Thus, there is strong motivation to identify the biology underlying psychosis risk in AD in hopes of developing a targeted, more efficacious intervention.

The risk for psychosis in AD is to a large extent genetically determined, with an estimated heritability of 60%, indicative of a distinct biologic vulnerability [4,11,12]. Because it has long been recognized that synapse loss is the strongest neuropathologic correlate of cognitive decline in AD,[13,14] it has been hypothesized that the vulnerability to AD + P arises from greater synaptic impairment in AD + P than AD-P. Prior studies that compared AD + P to AD-P subjects on a number of indirect markers of synapse integrity, including gray matter volumes, cerebral glucose utilization or blood flow, or gray matter concentrations of the membrane breakdown products, glycerophosphoethanolamine and glycerophosphocholine, have found support for this hypothesis across neocortical, but not medial temporal regions (reviewed in [15]). Most recently, we examined gray matter levels of a limited panel of 190 synaptic proteins in individuals with AD + P, finding reductions in canonical postsynaptic density (PSD) proteins relative to AD-P subjects [16]. These differences exceeded that which could be accounted for by any differences in neuropathology burden between the groups [16], or by reduction in the corresponding mRNA transcripts due to greater excitatory neuron loss in AD + P [17].

None of these prior studies have directly examined the PSD in AD + P. We therefore conducted a proteomic analysis of PSD fractions from dorsolateral prefrontal cortex of a large group of individuals with AD + P and AD-P, and a comparison group of cognitively normal elderly subjects. We found profoundly reduced levels of PSD proteins in AD + P relative to both AD-P and comparison subjects. PSDs from AD + P subjects had lower levels, relative to AD-P, for regulators of Rho GTPases and other proteins which regulate the actin cytoskeleton. Unlike AD + P, AD-P showed no global reduction of PSD protein levels relative to comparison subjects. Although, PSD protein changes in AD + P and AD-P relative to comparison subjects were highly correlated, the PSD of AD-P subjects was enriched, relative to comparison PSDs, for increased levels of proteins involved in protein isomerization and protein quality control, suggesting novel mechanisms of synaptic resilience in the AD-P cohort. Finally, we used the PSD protein level differences between AD + P and AD-P to nominate novel potential candidates for the treatment of AD + P.

Results

PSD abundance in AD with and without psychosis

To explore whether psychosis status globally affected the PSD in AD, we first evaluated the association of AD + P with total gray matter yield of PSD protein (Figure S1). Mean µg PSD/mg of gray matter was significantly reduced in AD + P vs AD-P ($t=-2.52$ $df = 119$ $p = 0.013$). PSD yield in AD + P was lower, and in AD-P higher, than in the elderly cognitively normal subjects, although neither of these latter differences was statistically significant.

PSD protein levels in AD with and without psychosis

Adjusted PSD protein levels are shown in Fig. 1. There was a significant shift of almost all proteins to lower levels in AD + P in comparison to AD-P ($t = -104$, $df = 1603$, $p < 2x10^{-322}$). We undertook several additional analyses to evaluate the robustness of this association. Down-regulation of protein levels in AD + P persisted when examining either the subset of 51 individuals who were included in our prior report of reduced levels of a targeted panel of 190 synaptic proteins[16], or the remaining 55 AD subjects who were newly evaluated (Figure S2A-C). Findings also persisted when evaluating the larger set of proteins resulting when using peptides quantified in at least 80% of samples (Figure S2D). We previously described excess reduction of excitatory neuron proportion in AD + P relative to AD-P in a cohort of 80 subjects, 76 of whom overlapped with the current analysis [17]. In those 76 subjects, including excitatory neuron proportion as a covariate did not eliminate the association of AD + P with lower PSD protein levels (Figure S2E-F).

Despite the overall shift in PSD protein abundance in AD + P relative to AD-P, no individual protein level was significantly reduced at a false discovery rate < 0.05 (Table S1). Functional annotation analysis of the 461 PSD proteins nominally significantly reduced in AD + P ($p < 0.05$) relative to a background of the 1604 proteins that were quantified revealed strong enrichment for regulators of the actin cytoskeleton, a

critical determinant of post-synaptic dendritic spine structure and function (Table 1). These included regulators of Rho GTPase signaling such as Pleckstrin homology domain containing Rho guanine nucleotide exchange factors (RhoGEFs) and Rho GTPase activating proteins (RhoGAPs). Additionally, a network of kinases that regulate these regulators and actin binding proteins were enriched in the set of proteins nominally significantly reduced in AD + P (Figure S3). Choice of a more liberal threshold for peptide inclusion (e.g. present call ≥ 80%) did not alter the functional annotation findings (Table S2).

The reduction in PSD protein abundance in AD + P relative to AD-P reflected a reduction of PSD protein levels in AD + P relative to elderly cognitively normal subjects, whereas there was no significant difference in PSD protein levels in AD-P relative to the elderly cognitively normal group (Fig. 2A-B). The protein whose abundance was most altered between the AD and comparison subjects was APP (Table S3), due solely to the increased levels of two peptides found within the Aβ sequence (RHDSGYEVHHQK and KLVFFAEDVGSNK). Overall, the protein alterations present in the two AD groups relative to elderly cognitively normal subjects were highly correlated (Fig. 2C). Nevertheless, functional annotation of the proteins that differentiated AD + P or AD-P from elderly cognitively normal subjects revealed differential patterns of enrichment. PSD proteins that differentiated AD + P from elderly cognitively normal subjects were primarily enriched for downregulated proteins involved in control of protein translation and synaptic proteins. PSD proteins that differentiated AD-P from elderly cognitively normal subjects were enriched for proteins involved in protein isomerization and protein quality control, with most of these having elevated levels in AD-P relative to comparison subjects (Table S4).

Relationship to genetic risk for AD with psychosis

We recently reported genome-wide gene-based tests of association with psychosis in AD [11]. 446 of the 461 PSD proteins that were nominally significantly reduced in AD + P had available corresponding gene-based tests of association (Table S5). Of these 446 genes whose proteins were assayed, 25 genes which were nominally altered at the protein level in AD + P also exhibited at least nominal evidence of genetic association with AD + P relative to AD-P (Table 2). Notable among these is *ENPP6*, a gene containing one of the two loci that were genome-wide significantly associated with psychosis risk in AD [11]. Also of interest were the actin binding protein genes *SYNPO*, *SYNE1*, *ALDOA*, and *VPS16*.

Predicted drug activity against the AD + P PSD protein network.

We identified 50 gene knockouts in which the resulting changes to the transcriptome were correlated with the PSD protein signature of AD + P (Table S6). For these genes, we further identified 32 drugs targeting them, 8 of which showed the desired effect (inhibitor/antagonist or positive regulator) at the targeted gene (Table 3). To further verify the potential post-treatment effect of the nominated drugs on PSD protein levels in AD + P, two additional analyses were performed. First the correlation of the regulator genes knockdown gene expression signature with just the 461 PSD proteins nominally significantly reduced in AD + P was assessed to ensure that the knockdown signature was not driven by the least dysregulated proteins. This analysis identified that MTOR had a correlation with the top 461 proteins that

was opposite (negative) to its overall correlation with the 1604 proteins, excluding it, and its positive regulator, pimecrolimus, from further consideration.

Second, we undertook to validate the gene signatures of the remaining candidate drugs. Of these, leronlimab, ibalizumab and epigallocatechin gallate were not found in the LINCS database for evaluation of their induced transcriptome expression signatures, and procaine was not tested in CNS cells. The remaining three medications, fostamatinib, odanacatib, and maraviroc all demonstrated transcriptome expression signatures that were negatively correlated with the AD + P PSD protein signature (Signed Jaccard Indexes of -0.0056, -0.0011, and − 0.0071, respectively, Table S7). These results compare favorably to those of our previous study that screened ~ 4000 drug-disease pairs, in which the average Signed Jaccard Index for drugs tested in a model of the disease for which it is indicated was − 0.0039 [39]. The current results for maraviroc and fostamatinib both showed scores with higher absolute values which are strong indicators for potential therapeutical effects.

Discussion

We hypothesized that AD + P is the result of a more severe synaptopathy than seen in AD-P, based on multiple studies that have compared indirect measures of synapse integrity both *in vivo* and in postmortem tissue, between AD + P and AD-P groups [15]. In the current report we provide the first direct comparison of the PSD between AD + P and AD-P subjects, finding severe disruption in the PSD proteome in association with psychosis in AD. Relative to AD-P, PSDs from AD + P subjects had lower levels of regulators of Rho GTPases and other proteins regulating the actin cytoskeleton. The PSD protein alterations in AD + P relative to AD-P were present within different subsets of study subjects and were not accounted for by altered burden of neuropathologies or the greater reduction in excitatory neurons that we have previously reported in AD + P relative to AD-P. Examining the pattern of PSD protein changes in AD + P and AD-P relative to cognitively normal elderly comparison subjects revealed additional insights. While both groups showed highly correlated PSD protein alterations relative to comparison subjects, AD-P subjects, unlike AD + P subjects, did not demonstrate an overall reduction in PSD protein abundance. In fact, the PSD of AD-P subjects was enriched, relative to comparison PSDs, for increased levels of proteins involved in protein isomerization and protein quality control, suggesting novel mechanisms of synaptic resilience in AD-P.

Given the prominent role post-synaptic regulation of the actin cytoskeleton plays in the maintenance and plasticity of dendritic spines [40], it is not surprising that the PSD proteome of AD + P was selective depleted of proteins enriched for functions associated with actin regulation. The identification of impairments of this signaling network provides a novel opportunity for identifying compounds that might have novel, specific therapeutic benefits for individuals with AD + P. We used a novel computational strategy, examining the overlap of gene knockout signatures with our AD + P PSD proteome alterations to identify upstream genes that could be pharmacologically targeted by existing compounds to potentially reverse the PSD proteome alterations in AD + P. The predictions we generated using this approach are subject to several limitations inherent in the available data used to generate them. Most studies reporting

the effects of gene knockdown rely on an assessment of the transcriptome, rather than the proteome, to characterize the effects of manipulation of these targets. These knockdown studies are most commonly conducted in cells and tissues of non-neuronal origin, and without exception do not assess the PSD. Although we utilized drug candidate signatures from studies obtained in CNS cells, we again relied on transcriptome, not proteome changes, and did not assess PSDs. As a result, our candidates will require validation in the PSD proteome of an intact neural model system. Additionally, we identified reductions in levels of a broad network of kinases. It is likely that not just PSD protein levels, but their phosphorylation state, are altered in AD + P. Thus, both delineation of the phosphoproteome signature of the AD + P PSD, and the impact of drug candidates upon this signature, remains needed.

Nevertheless, our strategy identified several genes that could represent novel targets for addressing the synaptic impairments in AD + P. For example, Cathepsin K (*CTSK*), which has been primarily studied for its role in bone metabolism, is expressed in neurons [41]. Germline knockout of *CTSK* leads to upregulation of some synaptic proteins, but is also associated with impaired learning and memory [41]. How a more moderate pharmacologic inhibition in adulthood would impact the PSD and cognition remains unknown. Aurora Kinase B, *AURKB*, has recently been shown to play a role promoting neurite formation during early neuronal development [42] and to promote axonal repair after injury in post-mitotic neurons [43]. Actin rod formation in neurons, which is promoted by agonism of the C-C Motif Chemokine Receptor 5, *CCR5*, has been increasingly recognized as a component of Alzheimer's neuropathology that induces PSD loss [44,45]. Although not specifically linked to inhibition of actin rod formation, the administration of CCR5 antagonists in a mouse model of AD reduced cognitive impairment [46]. Likewise, treatment with the CCR5 inhibitor, maraviroc, improved cognition in a small study of individuals with HIV-associated neurocognitive disorder [47].

Additional considerations apply in conceptualizing to prioritize among drug candidates at these targets. Repurposing a drug developed for treating other conditions makes it likely that off-target effects will be present and these may be detrimental. Ultimately any medication used will be applied to frail elderly individuals with multiple comorbidities, so preferred agents would be documented to be well-tolerated in such a population. Some of the medications we identified, e.g., fostamatinib, which was developed for chronic use in populations with serious autoimmune disease, and maraviroc, which was developed for chronic treatment of HIV infection, may well meet the tolerability benchmark [48,49]. For other identified agents in earlier stages of development, such as MV-711, further evidence is needed, but it should be noted that development of other CTSK inhibitors, including odanacatib, has been discontinued due to adverse events [50].

In our recent genome-wide association meta-analysis of over 12,000 AD subjects with or without psychosis, the most significant genetic locus associated with psychosis in AD was contained in a gene encoding ectonucleotide pyrophosphatase/phosphodiesterase 6 (ENPP6) [11]. We now report that ENPP6 is among the 461 PSD proteins with nominally reduced abundance in AD + P relative to AD-P. The expression of ENPP6 is selective for the oligodendrocyte lineage [51], peaking as oligodendrocyte precursor

cells (OPCs) differentiate into mature oligodendrocytes [52]. It has been established for some time that presynaptic terminals of excitatory neurons containing synaptic vesicles and release machinery align at electron-dense synaptic clefts abutting the processes of OPCs, and that the latter closely resemble the PSDs of dendritic spines, containing a postsynaptic membrane specialization and glutamate receptors (reviewed in[53]). Though not established, it is likely that these OPC PSDs are co-isolated with neuronal PSDs in our enrichment procedure. Others have demonstrated that synaptic input from glutamatergic neurons onto AMPA and NMDA receptors within the "PSDs" of oligodendrocytes regulate OPC proliferation and differentiation of OPCs to mature oligodendrocytes [54,55], a process during which ENPP6 expression is at its peak, and which is required for learning complex tasks [52]. Our finding of reduced ENPP6 abundance in the PSDs of AD + P would therefore suggest that activity dependent maturation of OPCs is impaired in AD + P relative to AD-P, and may contribute to the greater cognitive impairment in AD + P. Whether, and by what mechanism, this may relate to the genetic association of *ENPP6* with AD + P risk remains an open question.

We additionally identified an enrichment of genes encoding actin binding proteins, *SYNPO*, *SYNE1*, *ALDOA*, and *VPS16*, when we examined the overlap of the AD + P PSD proteome signature with genes nominated by our GWAS of AD + P. Two of these, *SYNPO* and *SYNE1*, are implicated in processes serving dendritic spine plasticity and maintenance, providing a link between the genetics of AD + P and its biologic signature of post-synaptic deficits. *SYNPO* encodes the protein synaptopodin, a dendritic spine protein that contributes to maintaining the long-term stability of large dendritic spines [56]. *SYNE1* encodes multiple actin-binding proteins via extensive alternative splicing. One of these proteins, candidate plasticity gene 2 (CPG2), which is transcribed from the region of *SYNE1* associated with risk for bipolar disorder [57], serves as a bridge between the dendritic spine endocytic machinery and the actin cytoskeleton necessary for activity dependent endocytosis of glutamate receptors [58]. *ALDOA* encodes the glycolytic enzyme Aldolase, Fructose-Bisphosphate A protein. While shown to promote lung cancer metastasis by interacting with gamma-actin [59], its role in neuronal function remans obscure. Of interest, however, given our computational predictions, ALDOA protein is found in actin rods [60]. *VPS16* encodes the VPS16 Core Subunit of CORVET and HOPS Complexes protein, which contributes to autophagosome-lysosome fusion. Mutations in *VPS16* cause dystonia syndromes, though the functions of *VPS16* in neurons, and the functional consequences of the identified mutations for neuronal and postsynaptic function are not currently established [61].

Individuals with AD-P showed a relative resilience to PSD protein loss, congruent with the widely replicated clinical observations that individuals with AD-P have slower cognitive and functional decline that individuals with AD + P. Our examination of where the PSD proteins that differentiated AD-P individuals from elderly cognitively normal subjects diverged from those of AD + P provides some potential insight into the source of this resilience. PSDs of AD-P subjects were enriched for upregulation of protein isomerases. Knowledge of how peptidyl-prolyl isomerases [62] and protein disulfide isomerases [63] may contribute to prevent tau fibril formation and the generation of Aβ is rapidly increasing. Many of the upregulated isomerases we identified have evidence that they may confer such protection (e.g. *PP1A*,

PTPA, *PDIA3*) [62,63]. *FKBP4* provides a more nuanced picture, as it may enhance tau fibrillization while protecting against Aβ generation [62]. For other upregulated isomerases we identified (GPI, PGAM1, MMUT, PTPA, PDIA3, FKBP4), no role in these processes is clearly identified.

We report the first study to directly interrogate the PSD in AD + P. Levels of most PSD proteins were substantially reduced in AD + P relative to both AD-P and comparison subjects. Examination of the PSD proteome signature of AD + P, relative to AD-P, subjects revealed lower levels of regulators of Rho GTPases, of multiple kinases, and of other regulators of the actin cytoskeleton, and served to nominate several novel potential pharmacotherapies for the treatment of AD + P. Future studies are required to further assess the ability of these drugs to impact the PSD proteome signature in animal and/or cellular models of Alzheimer disease.

Online Methods

Subjects

We studied 106 AD subjects (Table 4) obtained through the brain bank of the Alzheimer Disease Research Center (ADRC) at the University of Pittsburgh, using protocols approved by the University of Pittsburgh Institutional Review Board and Committee for Oversight of Research and Clinical Training Involving Decedents.

Cases with a primary neuropathologic diagnosis of Alzheimer's disease and a Braak stage between 3–5 were included in the study. End-stage cases, as defined by a Braak stage of 6, were excluded. Subjects underwent comprehensive evaluations by experienced clinicians in the ADRC, including neurologic, neuropsychological, and psychiatric assessments as previously described [16,17]. Using this information, information obtained from clinical records, and structured interviews with surviving relatives, an independent committee of experienced clinicians made consensus DSM-IV diagnoses for each subject. Psychosis was defined as the presence of delusions or hallucinations at any visit. Subjects with a preexisting psychotic disorder (e.g. schizophrenia) were excluded from the study.

Fixed and frozen tissue samples from 19 elderly cognitively normal comparison subjects from the Religious Order Study (ROS) were obtained from the Rush Alzheimer's Disease Center, along with basic demographic and neuropathologic information [18]. Mild neurodegenerative pathologic changes were accepted, up to a Braak stage of 2 for tau pathology, presence of sparse neuritic plaques or early TDP-43 pathology.

Sample collection and neuropathologic assessment

For ADRC subjects, postmortem interval (PMI) was recorded at the time of brain removal. At autopsy, the brain was removed intact, examined grossly, and divided in the midsagittal plane. Gray matter samples from the right superior frontal gyrus of the DLPFC were dissected and frozen at − 80°C. The left hemibrain was immersion fixed in 10% buffered formalin for at least one week, sectioned into 1.0 cm coronal slabs,

and sampled according to Consortium to Establish a Registry for Alzheimer's Disease (CERAD) protocol for neuropathological diagnosis of AD [19] or, since 2012, following National Institute of Aging – Alzheimer's Association (NIA-AA) guidelines [20]. AD pathology was evaluated using the modified Bielschowsky silver stain [21] and immunohistochemical staining for tau and amyloid β. Neuritic plaque density was assessed according to CERAD criteria [19]; distribution of tau pathology was classified according to Braak stages [22]. Lewy body pathology was assessed by alpha-synuclein immunohistochemistry, and positive cases were classified into amygdala-predominant, limbic/neocortical-predominant, or other categories, a modified scheme based on consensus criteria [20,23]. For analysis in this study, all alpha-synuclein positive categories were combined into one Lewy body positive group. Immunohistochemical staining for phospho-TDP-43 was performed on sections of amygdala, hippocampus, mesial temporal cortex and middle frontal gyrus as previously described [24]. Sections were evaluated for the absence or presence of TDP-43 positive neuronal cytoplasmic inclusions, neuronal intranuclear inclusions and dystrophic neurites. Based on the distribution of TDP-43 pathology, positive cases were classified into amygdala-predominant, mesial temporal, neocortical, or in cases when amygdala sections were not available, but all other sections were TDP-43 negative, indeterminate categories. For analysis in this study, all TDP-43 positive categories were combined into one TDP-43 positive group.

Assessment of vascular pathology included atherosclerosis of the circle of Willis, arteriolosclerosis in frontal white matter and cerebral amyloid angiopathy in DLPFC. Each was rated as none (0), mild (1), moderate (2) or severe (3), and a sum score was generated by adding the three individual scores. Microvascular lesions (MVL) were defined as remote microinfarcts/microhemorrhages not seen on gross examination and less than 1.0 cm in size. MVLs were enumerated in standardized sections [20] of middle frontal gyrus (DLPFC), superior and middle temporal gyrus, inferior parietal lobule, occipital cortex (BA 17/18), basal ganglia at level of anterior commissure, and thalamus at the level of the subthalamic nucleus to create MVL counts.

Neuropathologic diagnoses of Alzheimer disease were made according to CERAD criteria [19], although all AD subjects also met NIA-Reagan criteria [25] for intermediate to high probability that their dementia was due to AD lesions.

For the 19 elderly cognitively normal comparison subjects from the ROS, the same variables were provided to us, including Braak stage, CERAD neuritic plaque scores, presence/absence of TDP-43 and Lewy body pathologies, severity of vascular pathologies, and diagnostic classification based on modified CERAD and NIA-Reagan criteria (applying criteria in the absence of a diagnosis of dementia) [26].

Quantitative Immunohistochemistry

Serial 5 µm thick formalin-fixed, paraffin-embedded tissue sections were immunostained on an automated stainer (Discovery Ultra, Ventana, Tucson, AZ) using the following primary antibodies: PHF-1 (1:1000, kindly provided by Peter Davies), beta-amyloid NAB228 (1:4000 (Cell Signaling Technology,

Danvers, MA), after 40 min pretreatment with 90% formic acid), and microglial markers Iba1 (1:500, Wako, Richmond, VA) and HLA-DR (1:100, Dako, Agilent Technologies, Santa Clara, CA). Except for beta-amyloid, slides for all other stains were pretreated with Discovery CC1 solution, a Tris based buffer with a slightly basic pH (Ventana Medical Systems, Tucson, AZ). All slides were developed using a multimeric HRP/DAB detection system (Ventana Medical Systems, Tucson, AZ). No counterstaining was performed to ease signal quantification.

Microscopy

Whole slide digital images of the immunostained sections were created using a Mirax MIDI slide scanner (Zeiss, Jena, Germany) or Aperio AT2 slide scanner (Leica, Deer Park, IL) at 40x resolution. A subset of cases was scanned on both scanners to confirm very high concordance of digital image analysis results. Digital image analysis was performed using NearCyte software (Andrew Lesniak, University of Pittsburgh). For each section, 4 rectangular regions of interest (ROI) of 4mm^2 were created. These ROIs were defined to span the entire cortical thickness and were preferentially placed midway along the gyral axis to avoid tangentially cut cortical regions. Minor manual adjustments were made to adapt to curvatures and irregularities in the cortical ribbon. Once placed for the first analyzed stain (PHF-1), the same ROIs were re-used for all subsequent stains. If tissue folds or other artifacts prevented placement in the same location, the ROI was moved to an acceptable site as close as possible to the original location. For quantitative image analysis, thresholds for signal positivity were optimized manually for each stain and then maintained constant throughout the analysis of all slides. Signals from all four ROIs were integrated into two outcome variables: area ratio (= positive area/entire field area) and mean signal intensity. For HLA-DR and Iba1 stains, an additional variable, the HLA-DR/Iba1 ratio was derived to normalize microglial activation (HLA-DR) to microglial density (Iba1). All analyses were done blinded to psychosis status.

Biochemical Fractionation and LC-MS/MS

Prior to biochemical fractionation, subjects were stratified into blocks of 10–11 subjects, each block was balanced for diagnosis and sex. A post-hoc check also ensured that the distributions of PMI, age, age of AD onset, Braak stage and APOE*ε4 carrier status did not differ among all 12 blocks. PSD enrichments were generated using a variation on our previously describe approach [27]. Briefly, grey matter was homogenized in Syn-PER reagent (Thermo Scientific, Waltham, MA); synaptosomes were prepared according to manufacture protocol and washed with 1ml 0.1mM $CaCl_2$. The washed pellet was resuspended in 500 µl of 20 mm Tris pH 8.0 with 1% Triton X-100, agitated on a rocker at 4°C for 30min, and centrifuged at 47,000 RPM for 30 minutes at 4°C in the outer rim of a Sorval S80-AT2. The resulting pellet was washed with 250 µl 0.1mM $CaCl_2$ and centrifuged at 47,000 RPM for 30 minutes at 4°C. The washed PSD pellet was taken up in 50 µl 1X S-Trap Buffer (100mM TEAB, 5% SDS), vortexed and bath sonicated. Total protein concentration was determined by Micro-BCA (Thermo Scientific).

10 µg total PSD protein from each sample were reduced, alkylated, and trypsin digestion on S-Trap™ micro spin columns (ProtiFi) per manufacture protocol. Subject blocks were randomly assigned to TMT

blocks and labeled with TMTPro channels 1–11 as described in[28]. A pooled control was created using aliquots from the homogenate and synaptosome preparation steps which precede PSD generation (so as to save tissue resources). The pooled control was digested separately with S-Trap™ mini spin columns (ProtiFi, Farmingdale NY), split in two, and labeled with TMTPro channels 12 and 13. TMT labeled subject preparations from the same block were pooled along with 10 µg of the labeled pooled controls. The TMT labeled peptide pools were separated into eight fractions with the Pierce™ High pH Reversed-Phase Peptide Fractionation Kit (Thermo Scientific) per manufacture's protocol, evaporated, and reconstituted in 20 µl 97% H2O, 3% ACN, 0.1% formic acid.

~ 1 ug of TMT labeled peptides were loaded onto a heated PepMap RSLC C18 2 µm, 100 angstrom, 75 µm × 50 cm column (ThermoScientific) and eluted over 180 min gradients optimized for each high pH reverse-phase fraction as in[29]. Sample eluate was electrosprayed (2000 V) into a Thermo Scientific Orbitrap Eclipse mass spectrometer for analysis. MS1 spectra were acquired at a resolving power of 120,000. MS2 spectra were acquired in the Ion Trap with CID (35%) in centroid mode. Real-time search (RTS) (max search time = 34 s; max missed cleavages = 1; Xcorr = 1; dCn = 0.1; ppm = 5) was used to select ions for SPS for MS3. MS3 spectra were acquired in the Orbitrap with HCD (60%) with an isolation window = 0.7 m/z and a resolving power of 60,000, and a max injection time of 400 ms.

Raw MS files were processed in Proteome Discoverer version 2.5 (Thermo Scientific). MS spectra were searched against the *Homo sapiens* SwissProt database. SEQUEST search engine was used (enzyme = trypsin, max. missed cleavage = 2, min. peptide length = 6, precursor tolerance = 10ppm). Static modifications include acetylation (N-term, + 42.011 Da), Met-loss (N-term, -131.040 Da), Met-loss + Acetyl (N-temr, -89.030 Da), and TMT labeling (N-term and K, + 229.163 Da). Dynamic modification, oxidation (M, + 15.995 Da). PSMs were filtered by the Percolator node (max Delta Cn = 0.05, target FDR (strict) = 0.01, and target FDR (relaxed) = 0.05). Reporter ion quantification was based on corrected S/N values with the following settings: integration tolerance = 20ppm, method = most confident centroid, co-isolation threshold = 100, and SPS mass matches = 65.

Statistical Analysis

We performed rigorous QC and normalization on all quantified peptides. First, we performed sample loading normalization to make the total abundance the same across all samples. Second, peptides that were missing in both pooled control samples in at least half of the plexes were removed. We also removed peptides that were mapped to multiple proteins or genes. Next, an internal reference scaling (IRS) normalization[30] was performed for each peptide, where the scaling factor (for each plex) was calculated as the ratio of the overall mean of all pooled samples to the mean of the within-plex pooled samples. Finally, a median normalization was performed to make the median of each sample equal to the overall median of all samples.

To compare the PSD yield among three diagnosis groups, we performed linear regression adjusting for age, PMI, and sex. When comparing PSD yield among the two AD groups we additionally covaried for APOE*ε4 carrier status (which we have previously shown impacts the synaptic proteome in AD[31]) and for

Lewy body positivity and tau intensity (log2 transformed) as preliminary analyses revealed these two neuropathologies differed between the two AD groups. Then, for each sample, we multiplied the PSD yield to the normalized peptide abundance to account for the PSD yield variation in samples. Next, we performed PeCorA[32] analysis to identify “uncorrelated” peptides within each protein. In the end, we rolled up yield-adjusted peptide data to protein level by averaging the z-score of each peptide (on the log2 scale) that is mapped to the same protein. The “uncorrelated” peptides were treated as separate proteins and were not rolled up. We use different present call thresholds (e.g., 100%, 80%) when selecting peptides in the roll-up step.

Then we performed Limma[33,34] analysis for each yield-adjusted protein for our primary comparison of between AD + P and AD-P, adjusting age, PMI, sex, APOE*ε4 carrier status, Lewy body positivity, and tau intensity (log2 transformed). As a secondary analysis we compared AD + P, AD-P, and control, including age, PMI, and sex as covariates. APOE*ε4 carrier status and neuropathology variables were excluded from these comparisons as they are highly associated with diagnosis comparing AD and control. In all analyses two-group model-based log2 of fold change between any two groups was calculated for each protein.

Functional annotation analysis of differentially expressed proteins used DAVID[35]. In each analysis the differentially expressed proteins were tested for enrichment relative to a background of the 1604 proteins quantified in all samples.

Computational Systems Pharmacology

To identify medications with potential beneficial effects in treating AD + P, we conducted a series of systems pharmacology analyses. Since most significantly differentially expressed proteins were down-regulated in AD + P relative to AD-P, medications that directly target these proteins may have reduced efficacy due to the lower levels of the target. Therefore, we utilized a strategy designed to identify upstream targets that can regulate the activity of these differentially expressed proteins.

The data was analyzed with Illumina correlation engine (https://hsls.ce.basespace.illumina.com/c/nextbio.nb) and the knockdown atlas was used to identify genes which, when knocked down, altered expression of the mRNA corresponding to the 1604 proteins tested for differences between AD + P and AD-P. The identified genes (regulator-genes) were then extracted, as were the correlations of their knockdown transcriptome signature with the directions of alteration of the 1604 AD + P proteins.

We looked to identify medications that target the regulator-genes. Information about medications and their targets were extracted from DrugBank (https://www.drugbank.ca/)[36] including medication names, targets of medications and their corresponding actions. The desired drug-target action should be aligned with the correlation between regulator-gene knockdown and our dataset. For example, if a regulator-gene was negatively correlated with our dataset, it means that its knockout recapitulated many of the alterations we observed in AD + P relative to AD-P. Therefore, drugs that antagonize or otherwise inhibit its

activity would be predicted to induce a signal that can reverse the expression profile we observed in AD + P, which may lead to beneficial effects.

To confirm whether our identified drug candidates themselves would result in reversing the AD + P PSD proteome signature, we extracted the gene expression profile for each drug from Level 5 LINCS L1000 data [37], a collection of gene expression profiles for thousands of perturbagens at a variety of time points, doses, and cell lines (GEO database accession numbers: GSE70138 and GSE92742). The gene expression profiles were included only if they are from drug treatments on a cell line derived from the central nervous system and the drug dose was ≥ 1μM. To identify genes that are significantly differentially expressed, the Z scores from multiple tests for a same gene were averaged. An average $|Z|>1$ was considered a significant effect [38].

The association between drug and PSD data was quantitatively evaluated with Signed Jaccard Index [39]. The index ranges from + 1 to − 1, where + 1 and − 1 indicate the same, or inverse, pattern of two gene sets.

References

1. Ropacki SA, Jeste DV. Epidemiology of and risk factors for psychosis of Alzheimer's disease: a review of 55 studies published from 1990 to 2003. Am J Psychiatry. 11/2005 2005;162(11):2022–2030. Not in File.
2. Weamer EA, Emanuel JE, Varon D, et al. The relationship of excess cognitive impairment in MCI and early Alzheimer's disease to the subsequent emergence of psychosis. Int Psychogeriatr. 2/2009 Available online 9/25/2008 2009;21(1):78–85. Not in File.
3. Emanuel JE, Lopez OL, Houck PR, et al. Trajectory of cognitive decline as a predictor of psychosis in early Alzheimer disease in the cardiovascular health study. Am J Geriatr Psychiatry. 2/2011 2011;19(2):160–168. Not in File.
4. Sweet RA, Bennett DA, Graff-Radford NR, Mayeux R. Assessment and familial aggregation of psychosis in Alzheimer's disease from the National Institute on Aging Late Onset Alzheimer's Disease Family Study. Brain. 4/2010 2010;133(Pt 4):1155–1162. Not in File.
5. Schneider LS, Dagerman K, Insel PS. Efficacy and adverse effects of atypical antipsychotics for dementia: meta-analysis of randomized, placebo-controlled trials. Am J Geriatr Psychiatry. 3/2006 2006;14(3):191–210. Not in File.
6. Sweet RA, Pollock BG, Sukonick DL, et al. The 5-HTTPR polymorphism confers liability to a combined phenotype of psychotic and aggressive behavior in Alzheimer's disease. *International Psychogeriatrics*. 2001 2001;13(4):401–409. Not in File.
7. Kaufer DI, Cummings JL, Christine D, et al. Assessing the impact of neuropsychiatric symptoms in Alzheimer's disease: the Neuropsychiatric Inventory Caregiver Distress Scale. *J Am Geriatr Soc*. 1998 1998;46(2):210 – 15. Not in File.
8. Scarmeas N, Brandt J, Albert M, et al. Delusions and hallucinations are associated with worse outcome in Alzheimer disease. Arch Neurol. 10/2005 2005;62(10):1601–1608. Not in File.

9. Lopez OL, Wisniewski SR, Becker JT, Boller F, DeKosky ST. Psychiatric medication and abnormal behavior as predictors of progression in probable Alzheimer disease. *Arch Neurol*. 1999 1999;56(10):1266–1272. Not in File.
10. Wilson RS, Tang Y, Aggarwal NT, et al. Hallucinations, cognitive decline, and death in Alzheimer's disease. *Neuroepidemiology*. 2006 2006;26(2):68–75. Not in File.
11. DeMichele-Sweet MAA, Klei L, Creese B, et al. Genome-wide association identifies the first risk loci for psychosis in Alzheimer disease. Mol Psychiatry. Oct 2021;26(10):5797–5811. doi:10.1038/s41380-021-01152-8
12. Bacanu SA, Devlin B, Chowdari KV, DeKosky ST, Nimgaonkar VL, Sweet RA. Heritability of psychosis in Alzheimer disease. *American Journal of Geriatric Psychiatry*. 2005 2005;13(7):624–627. In File.
13. DeKosky ST, Scheff SW. Synapse loss in frontal cortex biopsies in Alzheimer's disease: Correlation with cognitive severity. *Ann Neurol*. 1990 1990;27:457–464. In File.
14. Terry RD, Masliah E, Salmon DP, et al. Physical basis of cognitive alterations in Alzheimer's disease: Synapse loss is the major correlate of cognitive impairment. *Ann Neurol*. 1991 1991;30:572–580. In File.
15. Murray PS, Kumar S, DeMichele-Sweet MA, Sweet RA. Psychosis in Alzheimer's Disease. *Biol Psychiatry*. 4/1/2014 2014;75(7):542–552. Not in File.
16. Krivinko JM, Erickson SL, Ding Y, et al. Synaptic Proteome Compensation and Resilience to Psychosis in Alzheimer's Disease. Am J Psychiatry. Oct 1 2018;175(10):999–1009. doi:10.1176/appi.ajp.2018.17080858
17. DeChellis-Marks MR, Wei Y, Ding Y, et al. Psychosis in Alzheimer's Disease Is Associated With Increased Excitatory Neuron Vulnerability and Post-transcriptional Mechanisms Altering Synaptic Protein Levels. Original Research. *Frontiers in Neurology*. 2022-March-02 2022;13doi:10.3389/fneur.2022.778419
18. Bennett DA, Buchman AS, Boyle PA, Barnes LL, Wilson RS, Schneider JA. Religious Orders Study and Rush Memory and Aging Project. J Alzheimers Dis. 2018;64(s1):S161-S189. doi:10.3233/JAD-179939
19. Mirra SS, Heyman A, McKeel D, et al. The consortium to establish a registry for Alzheimer's disease (CERAD). Part II. Standardization of the neuropathologic assessment of Alzheimer's disease. *Neurology*. 1991 1991;41:479–486. In File.
20. Montine TJ, Phelps CH, Beach TG, et al. National Institute on Aging-Alzheimer's Association guidelines for the neuropathologic assessment of Alzheimer's disease: a practical approach. Acta Neuropathol. 1/2012 2012;123(1):1–11. Not in File.
21. Yamamoto T, Hirano A. A comparative study of modified Bielschowsky, Bodian and thioflavin S stains on Alzheimer's neurofibrillary tangles. Neuropathol Appl Neurobiol. 1/1986 1986;12(1):3–9. Not in File.
22. Braak H, Alafuzoff I, Arzberger T, Kretzschmar H, Del TK. Staging of Alzheimer disease-associated neurofibrillary pathology using paraffin sections and immunocytochemistry. Acta Neuropathol.

10/2006 2006;112(4):389–404. Not in File.

23. McKeith IG, Dickson DW, Lowe J, et al. Diagnosis and management of dementia with Lewy bodies: third report of the DLB Consortium. Neurology. 12/27/2005 2005;65(12):1863–1872. Not in File.
24. Vatsavayi AV, Kofler J, DeMichele-Sweet MA, Murray PS, Lopez OL, Sweet RA. TAR DNA-binding protein 43 pathology in Alzheimer's disease with psychosis. *Int Psychogeriatr*. 3/4/2014 2014:1–8. Not in File.
25. Hyman BT, Trojanowski JQ. Consensus recommendations for the postmortem diagnosis of Alzheimer disease from the National Institute on Aging and the Reagan Institute Working Group on diagnostic criteria for the neuropathological assessment of Alzheimer disease. J Neuropathol Exp Neurol. 10/1997 1997;56(10):1095–1097. Not in File.
26. Bennett DA, Schneider JA, Arvanitakis Z, et al. Neuropathology of older persons without cognitive impairment from two community-based studies. Neurology. Jun 27 2006;66(12):1837–44. doi:10.1212/01.wnl.0000219668.47116.e6
27. Macdonald ML, Ciccimaro E, Prakash A, et al. Biochemical fractionation and stable isotope dilution liquid chromatography-mass spectrometry for targeted and microdomain-specific protein quantification in human postmortem brain tissue. Mol Cell Proteomics. 12/2012 2012;11(12):1670–1681. Not in File.
28. Zecha J, Satpathy S, Kanashova T, et al. TMT Labeling for the Masses: A Robust and Cost-efficient, In-solution Labeling Approach. Mol Cell Proteomics. Jul 2019;18(7):1468–1478. doi:10.1074/mcp.TIR119.001385
29. Dumrongprechachan V, Salisbury RB, Soto G, Kumar M, MacDonald ML, Kozorovitskiy Y. Cell-type and subcellular compartment-specific APEX2 proximity labeling reveals activity-dependent nuclear proteome dynamics in the striatum. Nat Commun. Aug 11 2021;12(1):4855. doi:10.1038/s41467-021-25144-y
30. Plubell DL, Wilmarth PA, Zhao Y, et al. Extended Multiplexing of Tandem Mass Tags (TMT) Labeling Reveals Age and High Fat Diet Specific Proteome Changes in Mouse Epididymal Adipose Tissue. Mol Cell Proteomics. May 2017;16(5):873–890. doi:10.1074/mcp.M116.065524
31. Sweet RA, Macdonald ML, Kirkwood CM, et al. Apolipoprotein E*4 (APOE*4) Genotype Is Associated with Altered Levels of Glutamate Signaling Proteins and Synaptic Coexpression Networks in the Prefrontal Cortex in Mild to Moderate Alzheimer Disease. Mol Cell Proteomics. 7/2016 2016;15(7):2252–2262. Not in File.
32. Dermit M, Peters-Clarke TM, Shishkova E, Meyer JG. Peptide Correlation Analysis (PeCorA) Reveals Differential Proteoform Regulation. J Proteome Res. Apr 2 2021;20(4):1972–1980. doi:10.1021/acs.jproteome.0c00602
33. Smyth GK. Linear models and empirical bayes methods for assessing differential expression in microarray experiments. Stat Appl Genet Mol Biol. 2004;3:Article3. doi:10.2202/1544-6115.1027
34. Ritchie ME, Phipson B, Wu D, et al. limma powers differential expression analyses for RNA-sequencing and microarray studies. Nucleic Acids Res. Apr 20 2015;43(7):e47.

doi:10.1093/nar/gkv007

35. Huang dW, Sherman BT, Lempicki RA. Systematic and integrative analysis of large gene lists using DAVID bioinformatics resources. *Nat Protoc*. 2009 2009;4(1):44–57. Not in File.
36. Wishart DS, Feunang YD, Guo AC, et al. DrugBank 5.0: a major update to the DrugBank database for 2018. Nucleic Acids Res. Jan 4 2018;46(D1):D1074-d1082. doi:10.1093/nar/gkx1037
37. Subramanian A, Narayan R, Corsello SM, et al. A Next Generation Connectivity Map: L1000 Platform and the First 1,000,000 Profiles. Cell. Nov 30 2017;171(6):1437–1452 e17. doi:10.1016/j.cell.2017.10.049
38. Stathias V, Jermakowicz AM, Maloof ME, et al. Drug and disease signature integration identifies synergistic combinations in glioblastoma. Nat Commun. Dec 14 2018;9(1):5315. doi:10.1038/s41467-018-07659-z
39. Qi X, Shen M, Fan P, et al. The Performance of Gene Expression Signature-Guided Drug-Disease Association in Different Categories of Drugs and Diseases. Molecules. Jun 16 2020;25(12)doi:10.3390/molecules25122776
40. Calabrese B, Wilson MS, Halpain S. Development and regulation of dendritic spine synapses. Physiology (Bethesda). 2/2006 2006;21:38–47. Not in File.
41. Dauth S, Sirbulescu RF, Jordans S, et al. Cathepsin K deficiency in mice induces structural and metabolic changes in the central nervous system that are associated with learning and memory deficits. BMC Neurosci. Jul 27 2011;12:74. doi:10.1186/1471-2202-12-74
42. Blazejewski SM, Bennison SA, Liu X, Toyo-Oka K. High-throughput kinase inhibitor screening reveals roles for Aurora and Nuak kinases in neurite initiation and dendritic branching. Sci Rep. Apr 14 2021;11(1):8156. doi:10.1038/s41598-021-87521-3
43. Gwee SSL, Radford RAW, Chow S, et al. Aurora kinase B regulates axonal outgrowth and regeneration in the spinal motor neurons of developing zebrafish. Cell Mol Life Sci. Dec 2018;75(23):4269–4285. doi:10.1007/s00018-018-2780-5
44. Bamburg JR, Minamide LS, Wiggan O, Tahtamouni LH, Kuhn TB. Cofilin and Actin Dynamics: Multiple Modes of Regulation and Their Impacts in Neuronal Development and Degeneration. Cells. Oct 12 2021;10(10)doi:10.3390/cells10102726
45. Cichon J, Sun C, Chen B, et al. Cofilin aggregation blocks intracellular trafficking and induces synaptic loss in hippocampal neurons. J Biol Chem. Feb 3 2012;287(6):3919–29. doi:10.1074/jbc.M111.301911
46. Gavriel Y, Rabinovich-Nikitin I, Ezra A, Barbiro B, Solomon B. Subcutaneous Administration of AMD3100 into Mice Models of Alzheimer's Disease Ameliorated Cognitive Impairment, Reduced Neuroinflammation, and Improved Pathophysiological Markers. J Alzheimers Dis. 2020;78(2):653–671. doi:10.3233/JAD-200506
47. Gates TM, Cysique LA, Siefried KJ, Chaganti J, Moffat KJ, Brew BJ. Maraviroc-intensified combined antiretroviral therapy improves cognition in virally suppressed HIV-associated neurocognitive disorder. AIDS. Feb 20 2016;30(4):591–600. doi:10.1097/QAD.0000000000000951

48. Weehuizen JM, Wensing AMJ, Mudrikova T, Wit F, Hoepelman AIM. Efficacy and safety of long-term maraviroc use in a heterogeneous group of HIV-infected patients: A retrospective cohort study. Int J Antimicrob Agents. Aug 2019;54(2):215–222. doi:10.1016/j.ijantimicag.2019.02.018
49. Tong S, Numerof RP, Datangel J, Masuda E. Long-Term Safety Profile of the Oral Spleen Tyrosine Kinase Inhibitor Fostamatinib in Immune Thrombocytopenia (ITP) and Other Diseases. Blood. 2020;136(Supplement 1):35–36. doi:10.1182/blood-2020-140907
50. Mullard A. Merck &Co. drops osteoporosis drug odanacatib. Nat Rev Drug Discov. Sep 29 2016;15(10):669. doi:10.1038/nrd.2016.207
51. Zhang Y, Chen K, Sloan SA, et al. An RNA-sequencing transcriptome and splicing database of glia, neurons, and vascular cells of the cerebral cortex. J Neurosci. Sep 3 2014;34(36):11929–47. doi:10.1523/JNEUROSCI.1860-14.2014
52. Xiao L, Ohayon D, McKenzie IA, et al. Rapid production of new oligodendrocytes is required in the earliest stages of motor-skill learning. Nat Neurosci. Sep 2016;19(9):1210–1217. doi:10.1038/nn.4351
53. Kula B, Chen TJ, Kukley M. Glutamatergic signaling between neurons and oligodendrocyte lineage cells: Is it synaptic or non-synaptic? Glia. Nov 2019;67(11):2071–2091. doi:10.1002/glia.23617
54. Gallo V, Zhou JM, McBain CJ, Wright P, Knutson PL, Armstrong RC. Oligodendrocyte progenitor cell proliferation and lineage progression are regulated by glutamate receptor-mediated K + channel block. J Neurosci. Apr 15 1996;16(8):2659–70.
55. Li C, Xiao L, Liu X, et al. A functional role of NMDA receptor in regulating the differentiation of oligodendrocyte precursor cells and remyelination. Glia. May 2013;61(5):732–49. doi:10.1002/glia.22469
56. Yap K, Drakew A, Smilovic D, et al. The actin-modulating protein synaptopodin mediates long-term survival of dendritic spines. Elife. Dec 4 2020;9doi:10.7554/eLife.62944
57. Rathje M, Waxman H, Benoit M, et al. Genetic variants in the bipolar disorder risk locus SYNE1 that affect CPG2 expression and protein function. Mol Psychiatry. Feb 2021;26(2):508–523. doi:10.1038/s41380-018-0314-z
58. Loebrich S, Benoit MR, Konopka JA, Cottrell JR, Gibson J, Nedivi E. CPG2 Recruits Endophilin B2 to the Cytoskeleton for Activity-Dependent Endocytosis of Synaptic Glutamate Receptors. Curr Biol. Feb 8 2016;26(3):296–308. doi:10.1016/j.cub.2015.11.071
59. Chang YC, Chiou J, Yang YF, et al. Therapeutic Targeting of Aldolase A Interactions Inhibits Lung Cancer Metastasis and Prolongs Survival. Cancer Res. Sep 15 2019;79(18):4754–4766. doi:10.1158/0008-5472.CAN-18-4080
60. Walter LM, Rademacher S, Pich A, Claus P. Profilin2 regulates actin rod assembly in neuronal cells. Sci Rep. May 13 2021;11(1):10287. doi:10.1038/s41598-021-89397-9
61. Steel D, Zech M, Zhao C, et al. Loss-of-Function Variants in HOPS Complex Genes VPS16 and VPS41 Cause Early Onset Dystonia Associated with Lysosomal Abnormalities. Ann Neurol. Nov 2020;88(5):867–877. doi:10.1002/ana.25879

62. Blair LJ, Baker JD, Sabbagh JJ, Dickey CA. The emerging role of peptidyl-prolyl isomerase chaperones in tau oligomerization, amyloid processing, and Alzheimer's disease. J Neurochem. Apr 2015;133(1):1–13. doi:10.1111/jnc.13033
63. Wang K, Liu JQ, Zhong T, et al. Phase Separation and Cytotoxicity of Tau are Modulated by Protein Disulfide Isomerase and S-nitrosylation of this Molecular Chaperone. J Mol Biol. Mar 27 2020;432(7):2141–2163. doi:10.1016/j.jmb.2020.02.013
64. Szklarczyk D, Franceschini A, Wyder S, et al. STRING v10: protein-protein interaction networks, integrated over the tree of life. Nucleic Acids Res. Jan 2015;43(Database issue):D447-52. doi:10.1093/nar/gku1003

Declarations

Acknowledgements, Funding Sources, and Conflicts: This work was supported by NIH grants R01 MH116046 (RAS, JK, LW) P30 AG066468 (OLL, RAS, JK), AG027224 (RAS), MH107756 (MLM), R03MH108849 (YD). The University of Pittsburgh holds a Physician-Scientist Institutional Award from the Burroughs Wellcome Fund which provided support to JMK. The ROS is supported by NIA grants P30AG10161, P30AG72975, and R01AG15819. ROS resources can be requested at:

https://urldefense.com/v3/__https://www.radc.rush.edu__;!!NHLzug!dzl-i9T2P7Yq0o71Lfqwa-cSaud9OpjBvjTsDe6tzNHRlKL4Oyl8PUqahO90pd4$

JMK, MRD, LZ, YD, MLM, OLL, LW, JK, and RAS have no biomedical financial interests or potential conflicts of interest to disclose. The content is solely the responsibility of the authors and does not necessarily represent the official views of the National Institute of Mental Health, the National Institutes of Health, or the United States Government.

Tables

Tables 1 and 2 are available in the supplementary files.

Table 3. Drugs with predicted beneficial effects.

Drug	Indication	Targets gene	Drug-target Action	Correlation Between Gene Knockdown Signature and AD+P PSD Protein Signature
Odanacatib	Osteoporosis	CTSK	Inhibitor	Negative
Fostamatinib	Chronic immune thrombocytopenia	AURKB	Inhibitor	Negative
Maraviroc	CCR5-tropic HIV-1 infection	CCR5	Antagonist	Negative
Leronlimab	Investigated for the treatment of a number of cancers and HIV	CCR5	Antagonist	Negative
Ibalizumab	HIV-1	CCR5	Antagonist	Negative
Procaine	Local anesthetic primarily in oral surgery	DNMT1	Inhibitor	Negative
Epigallocatechin Gallate	Investigated for the treatment of Hypertension and Diabetic Nephropathy.	DNMT1	Inhibitor	Negative
Pimecrolimus	Mild to moderate atopic dermatitis	MTOR	Potentiator	Positive*

*MTOR positively correlated with the entire AD+P PSD proteome signature (N=1604 proteins), but unlike the other target genes demonstrated an opposing pattern of correlations with the top differentially expressed PSD proteins (N=461).

Table 4. Subject Characteristics. Results are reported as “mean (SD)” or as “n (% of group total)”. ANOVA was performed for continuous variables with post-hoc Tukey’s test. Chi-square (or as appropriate Fisher’s exact) tests were performed for all categorical variables, pairwise post-hoc tests used Benjamini-Hochberg correction to adjust for multiplicity. The overall p values for the 3-group comparisons are shown. For all variables that were significantly different, AD+P and AD-P groups were each significantly different from elderly cognitively normal comparison subjects. AD+P and AD-P did not significantly differ from each other on any variable. *For Age of Onset and Duration of Illness p-values were generated using a two-sample sample t-test.

	AD - P (n=47)	AD + P (n=59)	Normal Comparison (n=19)	Overall p value
Age, years	84.4 (7.88)	83.7 (6.74)	84.5 (6.66)	0.826
Sex				
Male	19 (40.4%)	30 (50.8%)	6 (31.6%)	0.279
Female	28 (59.6%)	29 (49.2%)	13 (68.4%)	
PMI, hours	6.18 (3.73)	6.49 (4.22)	10.5 (6.63)	0.00163
Age of Onset, years	76.1 (8.33)	74.7 (7.03)		0.359
Duration of Illness, years	8.36 (3.63)	9.00 (3.25)		0.349
Braak Stage:				<0.001
0 - II	0 (0%)	0 (0%)	19 (100%)	
III	9 (19.1%)	5 (8.5%)	0 (0%)	
IV	19 (40.4%)	22 (37.3%)	0 (0%)	
V	19 (40.4%)	32 (54.2%)	0 (0%)	
APOE-4				0.00383
Positive	25 (53.2%)	35 (59.3%)	3 (15.8%)	
Negative	22 (46.8%)	24 (40.7%)	16 (84.2%)	
Antipsychotic Use				
Yes	4 (8.5%)	11 (18.6%)	0 (0%)	0.0595
No	43 (91.5%)	48 (81.4%)	19 (100%)	

Figures

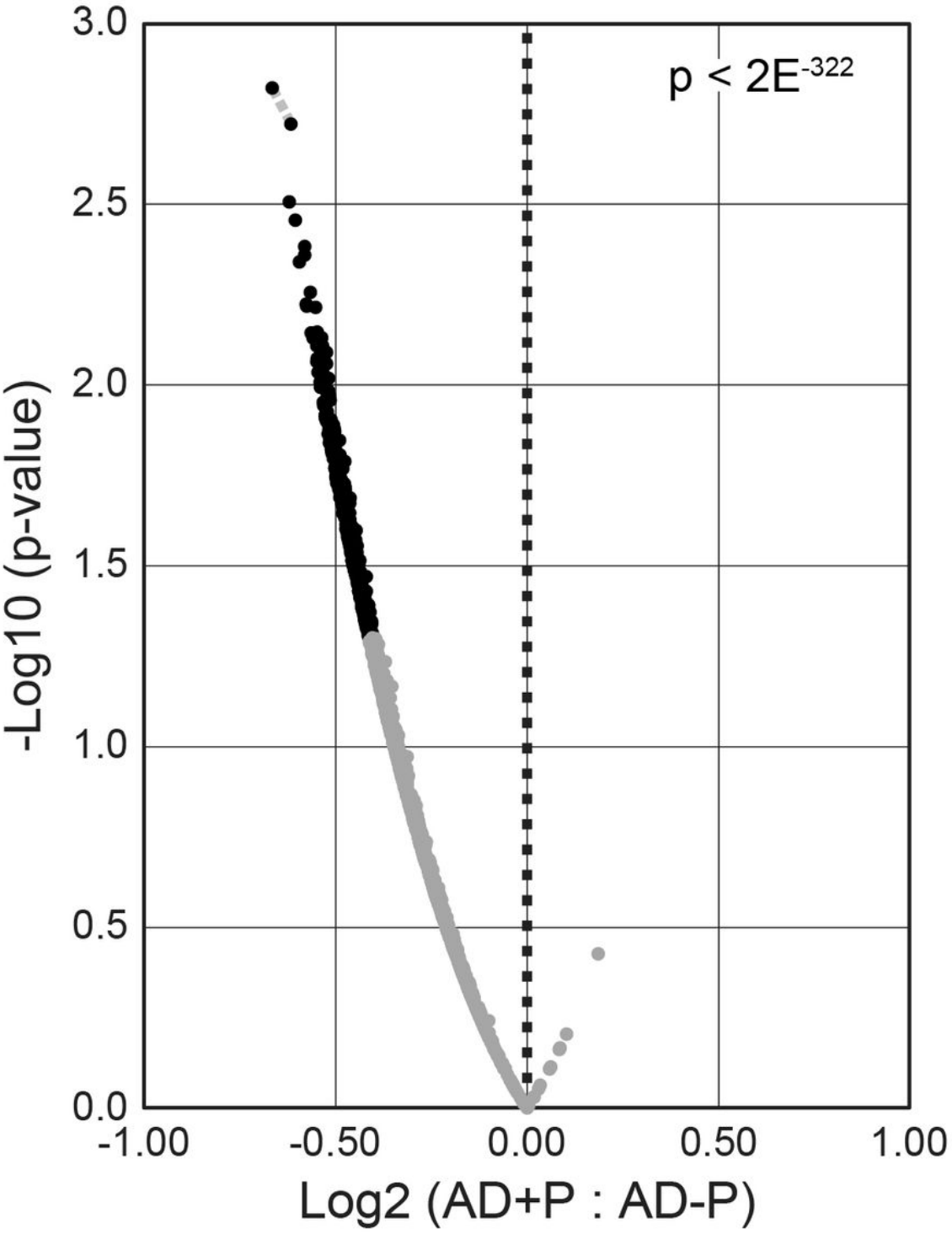

Figure 1

Distribution of levels of 1604 PSD proteins quantified in DLPFC using peptides present in 100% of AD+P and AD-P subjects. Distributions of $\log_2$ ratios are shown for all proteins, adjusted for covariates, Age, PMI, Sex, *APOE**E4, Lewy Body presence, and phosphor-Tau area fraction. The dashed vertical line represents no difference in the ratio of protein levels between groups. Black points indicate the 461

proteins with nominally significant differences in levels in AD+P relative to AD-P ($p<0.05$). AD+P is characterized by a significant shift towards lower PSD protein levels compared to AD-P.

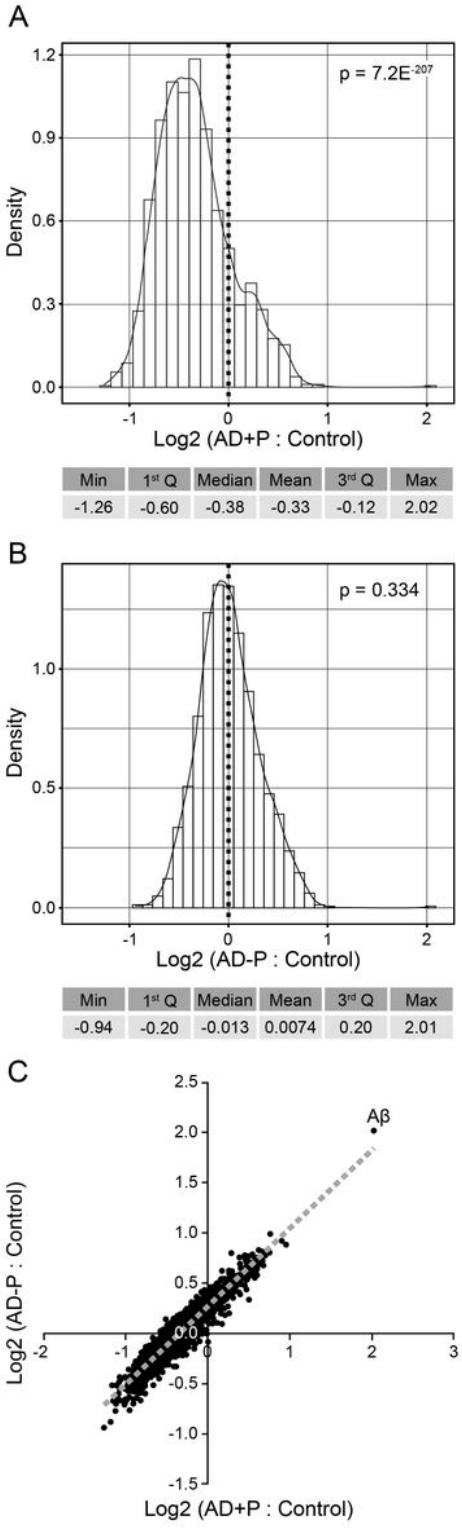

Figure 2

Distribution of levels of 1604 PSD proteins quantified in DLPFC using peptides present in 100% of AD+P and AD-P subjects relative to cognitively normal elderly comparison subjects. Distributions of $\log_2$ ratios

are shown for all proteins, adjusted for covariates, Age, PMI, and Sex. The dashed vertical line represents no difference in the ratio of protein levels between groups. AD+P is characterized by a significant shift towards lower PSD protein levels compared to Comparisons, whereas AD-P does not differ from comparison subjects.

Supplementary Files

This is a list of supplementary files associated with this preprint. Click to download.

- Table2.xlsx
- TableS7.xlsx
- FigureS1.jpg
- TableS4.xlsx
- FigureS2.jpg
- Table1.xlsx
- TableS2.xlsx
- TableS6.xlsx
- TableS5.xlsx
- TableS1.xlsx
- FigureS3.jpg
- TableS3.xlsx